Journal of Sound and Vibration 642 (2026) 119967

Contents lists available at ScienceDirect

Journal of Sound and Vibration

journal homepage: www.elsevier.com/locate/jsvi

From internal resonance to kinking and stacking in the response of nonlinear oscillators

Yannik Manz [a,b,*], André Gerlach [b], Norbert Hoffmann [a,c]

[a] Hamburg University of Technology, Institute for Structural Dynamics, Schloßmühlendamm 30, Hamburg, 21073, Germany
[b] Robert Bosch GmbH, Corporate Research, Robert-Bosch-Campus 1, Renningen, 71272, Germany
[c] Imperial College London, Mechanical Engineering, Exhibition Road, London, SW7 2AZ, UK

ARTICLE INFO

Keywords:
Kinking
Stacking
Nonlinear dynamics
Duffing oscillators
Frequency spacing
Internal resonance
Resonance overlap

ABSTRACT

In nonlinear dynamical systems, internal resonance is a well known phenomenon. Natural frequencies may change with vibration amplitude, becoming commensurable or close at certain energy levels. Nonlinear modes then interact based on their participating oscillators. Here, we investigate effects on the response curve of a system as neighboring oscillators are modified. This provides new insights into the relation of internal resonance and the frequency response of coupled nonlinear systems. We use methods of Harmonic Balance and a continuation algorithm to compute nonlinear frequency response curves and nonlinear normal modes for a model system. It is arranged as a chain of Duffing oscillators with separated natural frequencies. We demonstrate a kinking effect in the response curve once internal resonance emerges in the system's forced response. The kink is observed as a shift to higher response levels, stretching the response curve. We also show how this kinking effect is modified by adapting the nonlinearities of neighboring oscillators. The system's response branches kink vertically as an oscillator in the chain is made linear, stacking on top of each other. Multiple stable solutions at a certain frequency may then be observed. We show that these solutions correspond to varying degrees of vibration localization in the system. We expect our results to be valuable in system design. It should be possible to exploit the observed kinking effect, shaping the response curve by adding suitable oscillators of various characteristics. The engineer may thus be able to reach a target system response level at a certain frequency.

1. Introduction

In nonlinear dynamical systems, it is well known that natural frequencies may vary with vibration amplitude [1]. A popular example is the Duffing oscillator, whose natural frequency is a function of amplitude due to a cubic stiffness term included in the nonlinear restoring force [2]. In a system of coupled oscillators, natural frequencies may then become equal or commensurable at certain energy levels. This is known as (nonlinear) internal resonance [1,3]. It is accompanied by nonlinear modal interaction, governed by the properties of the participating oscillators.

In this paper, we examine the influence of neighboring oscillators on the response curve of a system. A chain of nonlinear Duffing oscillators is used, their natural frequencies are separated. As internal resonance emerges in the forced response of the system, we observe a kinking effect. The response curve shows a bend, altering its response level. The curve then looks stretched. We demonstrate

* Corresponding author.
E-mail address: yannik.manz@tuhh.de (Y. Manz).

https://doi.org/10.1016/j.jsv.2026.119967
Received 18 February 2026; Received in revised form 17 June 2026; Accepted 21 June 2026
Available online 23 June 2026
0022-460X/

how this effect is modified by manipulation of neighboring oscillators' nonlinearities. Introducing a linear oscillator in the chain results in vertical kinking of the system's response branches. This is reflected in an increase of the response level while maintaining a certain frequency. Multiple response branches can here overlay on top of each other, creating a stacking effect in the response curve. In such a scenario, multiple solutions may be found at a certain frequency. We demonstrate that these solutions correspond to localized vibration patterns. Further modification of an oscillator's nonlinearity reveals a limiting effect on the frequency attainable by the system's response branches. In a zone of internal resonance, response branches may self-intersect as they bend. We demonstrate that the system response can overcome this region as excitation amplitude is increased.

Internal resonance in the context of coupled nonlinear systems is investigated in various fields. Research has been done in the context of beams and plates [4–10]. Micro- and nanoelectromechanical systems (MEMS/NEMS) are known to exhibit internal resonance behavior [11–15]. Effects arising from nonlinear modal interactions are investigated and utilized to manipulate the system behavior [16–21]. Recently, the focus has been on energy harvesting and vibration mitigation technology, where internal resonances are exploited to influence energy transfer as modes interact [22–25]. Various lumped-parameter models are also routinely employed in the investigation of nonlinear dynamical systems [26–30]. Properties of included oscillators can be readily examined in these systems. Such research often uses systems explicitly created to exhibit internal resonance, for example by introducing commensurability of their natural frequencies [4,31–33]. A special case in this context is the symmetric system (e.g., a chain of equal Duffing oscillators), where internal 1:1 resonance is present by default [13,28,34–36]. We intend to expand the existing perspectives on the interaction of coupled oscillators, providing new insights into the dynamics at play. We focus our work on the relation between internal resonance and the system's frequency response as neighboring oscillators are modified.

This paper is structured as follows: In Section 2, we set up the framework for our model and introduce the methods used. Section 3 presents the results of the investigation as the model's properties are modified, catching kinking and stacking phenomena in the system response. Section 4 then discusses the results and motivates further research based on our findings.

2. Methods and model

We investigate a system of coupled nonlinear oscillators. Their linear natural frequencies are separated and initially not commensurable. We focus on the computation of periodic steady state solutions to the system. We apply the well-established method of Harmonic Balance (HBM) to obtain periodic solutions of the nonlinear system. A continuation scheme is used to track solutions through the evolution of a parameter. Hill's method is used to assess stability of the solutions.

2.1. Model: A chain of duffing oscillators

Consider a system of Duffing oscillators, cyclically connected to each other by a coupling spring k_c to form a chain as shown in Fig. 1. Each oscillator of mass m is connected to ground by a viscous damper d and a linear spring k. A nonlinear force acts on each oscillator due to a nonlinear stiffness k_{nl}. An external excitation $f(t)$ is applied, dependent on time t. Such a system may be used, for example, as a minimal model for aerospace engineering structures undergoing large deformations, such as turbine blisks [34,37–39]. Similar systems may also be used to model interconnected components at various levels of wear within large machinery [40,41]. The equation of motion for the n-th oscillator is

$$m_n\ddot{x}_n + d_n\dot{x}_n + k_n x_n + k_{\mathrm{nl},n}x_n^3 + k_{\mathrm{c},n}\left(2x_n - x_{n-1} - x_{n+1}\right) = f_n(t), \tag{1}$$

where x is the oscillator displacement from the equilibrium position of the system and $\dot{x} = \frac{\mathrm{d}x}{\mathrm{d}t}$, $\ddot{x} = \frac{\mathrm{d}^2x}{\mathrm{d}t^2}$ are velocity and acceleration, respectively. Eq. (1) is mass-normalized to give

$$\ddot{x}_n + 2\zeta_n\omega_{0n}\dot{x}_n + \omega_{0n}^2 x_n + \gamma_n x_n^3 + \omega_{\mathrm{c},n}^2\left(2x_n - x_{n-1} - x_{n+1}\right) = \frac{f_n(t)}{m_n}. \tag{2}$$

Here, $\zeta_n = \frac{d_n}{2\sqrt{m_n k_n}}$, $\omega_{0n}^2 = \frac{k_n}{m_n}$, $\gamma_n = \frac{k_{\mathrm{nl},n}}{m_n}$ and $\omega_{\mathrm{c},n}^2 = \frac{k_{\mathrm{c},n}}{m_n}$. We introduce a new time scale $\tau = \omega_{\mathrm{ref}}t$, where $\omega_{\mathrm{ref}} = \sqrt{\frac{k_{\mathrm{ref}}}{m_{\mathrm{ref}}}}$ may be set to any of the linear natural frequencies ω_{0n}. Scaling the displacement by $x_n(t) = X_0 u_n(\tau)$, the non-dimensional form of the nonlinear differential equation at oscillator n is obtained as

$$u_n'' + 2\xi_n u_n' + \eta_n^2 u_n + \beta_n u_n^3 + \kappa_n^2(2u_n - u_{n-1} - u_{n+1}) = g_n(\tau), \tag{3}$$

where the prime denotes a derivative with respect to dimensionless time τ, $\xi_n = \zeta_n\frac{\omega_{0n}}{\omega_{\mathrm{ref}}}$ is a dimensionless damping ratio, $\eta_n^2 = \frac{\omega_{0n}^2}{\omega_{\mathrm{ref}}^2}$ is a linear natural frequency ratio, $\beta_n = \frac{\gamma_n}{\omega_{\mathrm{ref}}^2}X_0^2$ defines the nonlinearity, $\kappa_n^2 = \frac{\omega_{\mathrm{c},n}^2}{\omega_{\mathrm{ref}}^2}$ is the coupling ratio and $g_n(\tau) = \frac{f_n(t)}{m_n\omega_{\mathrm{ref}}^2 X_0}$ is a dimensionless excitation force. Throughout this paper, harmonic excitation of the form $f_n(t) = \hat{f}_n\cos\left(\Omega t + \phi_0\right)$ is assumed. Setting the initial phase $\phi_0 = 0$, we get

$$g_n(\tau) = \hat{g}_n\cos(\omega\tau) \tag{4}$$

with excitation amplitude $\hat{g}$ and excitation frequency $\omega = \frac{\Omega}{\omega_{\mathrm{ref}}}$. Cyclic boundary conditions will be imposed such that, in a system of N oscillators, $u_{N+1} = u_1$ and $u_0 = u_N$. Note that for the special case of $N = 2$ oscillators, this constraint results in the use of two coupling springs. Such a setup simplifies scaling to larger models, retaining consistency.

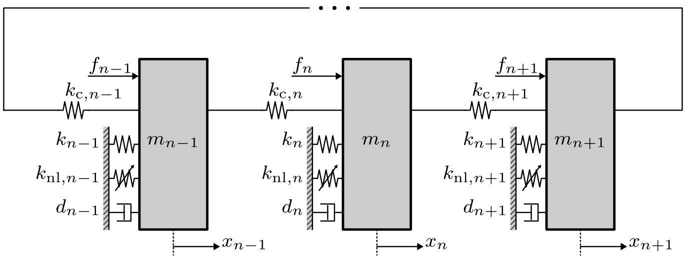

Fig. 1. Model system, set up as a chain of Duffing oscillators with cyclic nearest-neighbor coupling. The figure shows a subset of the model, visualizing the coupling.

2.2. Method of harmonic balance

The equation of motion of the dynamical system (cf. Eq. (3)) may be rewritten as

$$\mathbf{I}\mathbf{u}'' + \boldsymbol{\Xi}\mathbf{u}' + \boldsymbol{\Lambda}\mathbf{u} + \mathbf{g}_{\mathrm{nl}}(\mathbf{u}, \mathbf{u}') = \mathbf{g}_{\mathrm{exc}} \ , \tag{5}$$

where $\mathbf{I}$ is the identity matrix, $\boldsymbol{\Xi}$, $\boldsymbol{\Lambda}$ denote the nondimensional damping ratio and stiffness ratio matrices, respectively, $\mathbf{u}$ is a vector of system coordinates and $\mathbf{g}_{\mathrm{exc}}$ is a vector of periodic excitation forces applied to the corresponding coordinates. Nonlinear forces are described by a vector $\mathbf{g}_{\mathrm{nl}}$ and may be, in general, conservative or non-conservative.

We search for periodic solutions to Eq. (5) by approximation with a truncated Fourier series. We write

$$\mathbf{u}(\tau) \approx \bar{\mathbf{u}}_0 + \sum_{h=1}^{H} \bar{\mathbf{u}}_{\mathrm{c},h} \cos(h\omega\tau) + \bar{\mathbf{u}}_{\mathrm{s},h} \sin(h\omega\tau) \ , \tag{6}$$

where H is the truncation order, $\omega = 2\pi/T$ is the fundamental oscillation frequency with period T, $\bar{\mathbf{u}}_0$ is the mean value of the function over one period and $\bar{\mathbf{u}}_{\mathrm{c},h}$, $\bar{\mathbf{u}}_{\mathrm{s},h}$ are the Fourier coefficients corresponding to the cosine and sine parts of harmonic h:

$$\bar{\mathbf{u}}_0 = \frac{1}{T}\int_{-T/2}^{T/2} \mathbf{u}(\tau)\mathrm{d}\tau, \tag{7}$$

$$\bar{\mathbf{u}}_{\mathrm{c},h} = \frac{2}{T}\int_{-T/2}^{T/2} \mathbf{u}(\tau)\cos(h\omega\tau)\mathrm{d}\tau, \tag{8}$$

$$\bar{\mathbf{u}}_{\mathrm{s},h} = \frac{2}{T}\int_{-T/2}^{T/2} \mathbf{u}(\tau)\sin(h\omega\tau)\mathrm{d}\tau \ . \tag{9}$$

Substituting Eq. (6) into (5) and projecting the resulting equations on the Fourier basis 1, $\cos(\omega\tau)$, $\sin(\omega\tau)$ yields an algebraic set of nonlinear equations. The residual $\bar{\mathbf{r}}$ is required to become zero for the Fourier coefficients up to truncation order H [3]:

$$\bar{\mathbf{r}}(\bar{\mathbf{u}}, \omega) = \mathbf{S}(\omega)\bar{\mathbf{u}} + \bar{\mathbf{g}}_{\mathrm{nl}}(\bar{\mathbf{u}}, \omega) - \bar{\mathbf{g}}_{\mathrm{exc}}(\omega) = \mathbf{0} \ . \tag{10}$$

Here, $\bar{\mathbf{u}}$ is a vector collecting the Fourier coefficients $\bar{\mathbf{u}}_{\mathrm{c},h}$, $\bar{\mathbf{u}}_{\mathrm{s},h}$, $\mathbf{S}(\omega)$ is the dynamic stiffness matrix in frequency domain, $\bar{\mathbf{g}}_{\mathrm{exc}}(\omega)$ represent the Fourier coefficients of the external excitation and $\bar{\mathbf{g}}_{\mathrm{nl}}(\bar{\mathbf{u}}, \omega)$ those of the nonlinear forces within the system. The latter are evaluated using an alternating frequency-time method (AFT). Details on the AFT may be found in, e.g., [3]. The resulting number of algebraic equations to be solved is $N(2H + 1)$. Providing an initial guess based on steady state solutions obtained from a time integration algorithm, a Newton-Raphson scheme is used to search for solutions. Numerical path continuation is employed to track the evolving solutions as a parameter is varied. This allows for following an arbitrary curve in parameter space [42–44]. We use a predictor-corrector scheme with tangent predictor and arc-length parametrization to find appropriate solutions as the parameter is evolved. Various other variants of continuation algorithms are available; an overview is given in [3]. Implementations of continuation algorithms in the context of dynamical systems and the analysis of bifurcations are available in various software packages such as, for example, AUTO [45], MatCont [46] and MANLAB [47].

We use HBM and continuation for two purposes: calculation of nonlinear frequency response curves (NFRCs) and of nonlinear normal modes (NNMs). Both are established procedures in the analysis of nonlinear dynamical systems. The interested reader is referred to [1,3,48] for a detailed introduction, [49–54] for underlying principles and [31,55] for computational aspects. Computation of the NNMs is performed on the free and conservative system, neglecting excitation as well as the velocity proportional damping term in Eq. (5). Periodic solutions are then obtained using an additional phase constraint in the continuation algorithm. The obtained Fourier coefficients are used to compute the system response. We investigate the system dynamics based on its overall response level. The L^2-norm of the system is calculated as

$$L^2 = \sqrt{\sum_{n=1}^{N}\sum_{l=0}^{H}\left(\bar{u}^2_{\mathrm{c},n,l} + \bar{u}^2_{\mathrm{s},n,l}\right)} \ , \tag{11}$$

where $\bar{u}_{c,n,l}$, $\bar{u}_{s,n,l}$ are the Fourier coefficients at harmonic index l (including the mean value term for $l = 0$) of degree-of-freedom n. The L^2-norm may be viewed as a *fictitious energy measure* of the system; it does not, however, correspond to the time varying vibration energy of the system, as the varying phase differences of the oscillator vibrations are not considered.

2.3. Stability analysis

The continuation procedure using HBM gives no indication on the stability of a computed periodic solution. In time-domain methods, the monodromy matrix of a system is used for that purpose. Stability can be deduced from its eigenvalues, termed Floquet multipliers [42]. An analogous procedure in frequency domain is called Hill's method. It may be applied together with HBM to assess stability. We give a short summary of Hill's method here. Detailed introductions may be found in, e.g., [3,56,57].

Hill's method transforms a linear time-variant system into a time-invariant eigenvalue problem via Fourier expansion. In order to apply this approach to nonlinear systems, linearization around a solution point is employed [56]. A periodic solution $\mathbf{u}^*(\tau) = \mathbf{u}^*(\tau + T)$ is perturbed by a function $\mathbf{p}(\tau)$, consisting of a periodic term $\mathbf{s}(\tau)$ modulated by an decay term $\exp(\sigma\tau)$. The perturbed expression reads

$$\mathbf{u}(\tau) = \mathbf{u}^*(\tau) + \mathbf{p}(\tau) = \mathbf{u}^*(\tau) + \mathbf{s}(\tau)\exp(\sigma\tau). \tag{12}$$

Eq. (12) is substituted into the equations of motion of the system, cf. Eq. (5). The solution as well as the perturbation are approximated as truncated Fourier series and a projection step as in Section 2.2 is applied. After linearization around the periodic solution $\mathbf{u}^*(\tau)$, a quadratic eigenvalue problem in frequency domain is obtained:

$$\left[\boldsymbol{\Delta}_2\sigma^2 + \boldsymbol{\Delta}_1\sigma + \boldsymbol{\Delta}_0\right]\bar{\mathbf{s}} = \mathbf{0}, \tag{13}$$

where $\bar{\mathbf{s}}$ is the vector of Fourier coefficients of the perturbation's T-periodic part $\mathbf{s}(\tau)$. For our model, $\boldsymbol{\Delta}_0$ is the derivative matrix of the residual $\bar{\mathbf{r}}$ at the periodic solution point, $\boldsymbol{\Delta}_0 = \partial\bar{\mathbf{r}}/\partial\bar{\mathbf{u}}\big|_{\bar{\mathbf{u}}^*}$. The coefficient matrices $\boldsymbol{\Delta}_1$, $\boldsymbol{\Delta}_2$ describe the system dynamics; they are given in Appendix A. For a detailed derivation of Eq. (13) and the corresponding coefficient matrices, the reader is referred to, e.g., [57]. Eq. (13) yields $(2H + 1)2N$ eigenvalues, of which only $2N$ eigenvalues approximate the Floquet exponents $\tilde{\boldsymbol{\sigma}}$. The remaining eigenvalues are spurious, introduced through truncation of the Fourier series. A filtering technique has to be applied to the set of eigenvalues to obtain the Floquet exponents. A practical approach is filtering by minimal distance to the real axis [58]. The Floquet exponents are thus

$$\tilde{\boldsymbol{\sigma}} = \left[\sigma_{(l)}\right]_{l=1}^{2N}, \text{ with } \left|\mathrm{Im}(\sigma_{(1)})\right| \leq \left|\mathrm{Im}(\sigma_{(2)})\right| \leq \ldots \leq \left|\mathrm{Im}(\sigma_{(2N)})\right|. \tag{14}$$

They relate to the Floquet multipliers $\tilde{\boldsymbol{\lambda}}$ through

$$\tilde{\lambda}_l = \exp(\tilde{\sigma}_l T). \tag{15}$$

Stability is indicated by the real parts of all Floquet exponents being negative. Otherwise, at least one positive real part indicates an unstable solution.

In addition to general stability analysis, the Floquet exponents may be used for the detection of bifurcations. A common method is tracking sign changes of the Floquet exponents' real parts. If a real-valued Floquet exponent crosses the imaginary axis, a bifurcation is detected, associated with a change of stability. If the corresponding Floquet multiplier leaves the unit circle at $+1$, a fold bifurcation is found; period-doubling is encountered if the Floquet multiplier leaves the unit circle at -1. A pair of complex-valued exponents crossing the imaginary axis indicate a change of stability through a Neimark-Sacker bifurcation. Here, the system branches to/from a torus [42]. Next to the tracking of Floquet exponents, test functions can be evaluated to assess bifurcation behavior. For an overview on test functions, the reader is referred to [42]. Details on implementation can be found in, e.g., [46,57,59].

2.4. Computational aspects and parameters used in this study

Numerical computation is performed using a modified version of the free software package *NLvib* [3]. All simulations are run in *MATLAB R2024b* [60]. The parameters listed in Table 1 are used throughout this study, unless stated otherwise. They are chosen to resemble a model used in [34], where a symmetric setup was enforced (i.e., $\eta_n^2 = 1$ was chosen for all n). We emphasize the setup of the frequency ratio η_n^2 in our model: The oscillator with the lowest frequency is used as a reference. Subsequent oscillators have their frequencies spaced equally, controlled by frequency spacing constant a.

3. Results

3.1. Reducing frequency spacing between two nonlinear oscillators: Resonance overlap and response branch kinking

In this section, we investigate the effect the linear natural frequency spacing has on the nonlinear frequency response curve of our system. We initially set up the system with two oscillators and far-spaced frequencies, $a = 1.2$, as shown in Fig. 2a (blue curve). The response shows two distinct resonance branches, each bending towards higher frequencies as the amplitude is increased. As the first oscillator's resonance is passed, its maximum resonance frequency (that is, the highest frequency attained as the response branch bends due to the hardening effect) remains lower than the initial resonance frequency of the second oscillator. There remains a frequency gap where neither oscillator is in resonance. Next, the frequency spacing is decreased, first setting $a = 0.7$, then $a = 0.3$. Fig. 2a shows the corresponding effect in the system response: The frequency gap between the two resonances vanishes. The second

Table 1
Overview of the parameters used in this study, unless stated otherwise. Weak coupling is implemented, the oscillators are weakly damped.

Measure	Symbol	Value
damping ratio	ξ_n	0.005
frequency ratio	η_n^2	$1 + a(n-1)$
frequency spacing constant	a	0.3
nonlinear factor	β_n	1
coupling ratio	κ_n^2	0.01
excitation amplitude	$\hat{g}_n$	0.012
truncation order	H	9

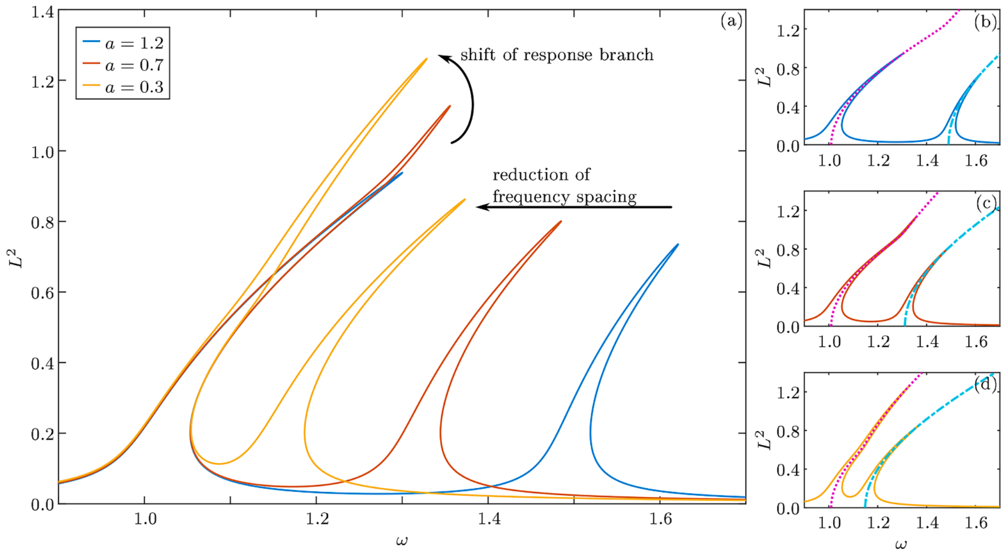

Fig. 2. Effect of frequency spacing on the system response for $N = 2$ oscillators. L^2-norm is used to measure the response level, cf. Eq. (11). **(a)** Nonlinear frequency response curves for three different frequency spacing values. A kink in the first response branch is observed as the natural frequency spacing is reduced. **(b)**, **(c)**, **(d)** Three separate panels show the different NFRCs and the corresponding nonlinear normal modes. NNM 1 is shown as a dotted line (color: magenta), NNM 2 as a dashed-dotted line (color: cyan).

oscillator's resonance sets on even as the response branch from driving through the first oscillator's resonance is still bending towards its maximum. We term this "resonance overlap" and observe an interesting effect on the response curve. The upper response branch shows an upward kink. This means that the response curve shifts to larger response levels, making the overall response curve look bent and stretched. Looking at the NFRC for close frequency spacing, $a = 0.3$, we observe a similar effect. It is setting on at a lower frequency, corresponding to a lower resonance frequency of the second oscillator.

Reducing frequency spacing thus may lead to resonance overlap in the response curve. This overlap is accompanied by a kink in the response branch. The frequency location of the kink relates to the onset of a neighboring oscillator's resonance.

3.2. Nonlinear normal modes and internal resonance

We next check whether the observed kink can be related to the neighboring oscillator's natural frequency. We calculate the nonlinear normal modes of the system and overlay them in the response graphs. They represent the backbone curves of the resonances. The corresponding graphs are shown in Figs. 2b–d. We observe distinct kinks in the NNMs for medium and small frequency spacing (Figs. 2c, 2d). As NNM 1 bends over the low amplitude natural frequency of NNM 2, internal 1:1 resonance occurs. This relates to the observed kink in the forced response as the modes interact. Note that for far-spaced frequencies (cf. Fig. 2b), the NNMs also exhibit a kink where the two modes reach internal 1:1 resonance. We do not see this in the system response as the excitation is not strong enough to drive the response in resonance further up on the backbone curve. One would expect the forced response to reach this point if the excitation amplitude is increased or if damping is reduced. Resonance overlap would then be observed in the response, and the NNM's kink would emerge as a kink of the response curve.

We have shown that the kink in the system response is related to internal 1:1 resonance. It can be observed in the NNMs and relates to the onset of the neighboring vibration mode. Resonance overlap then makes this phenomenon visible in the system's frequency response.

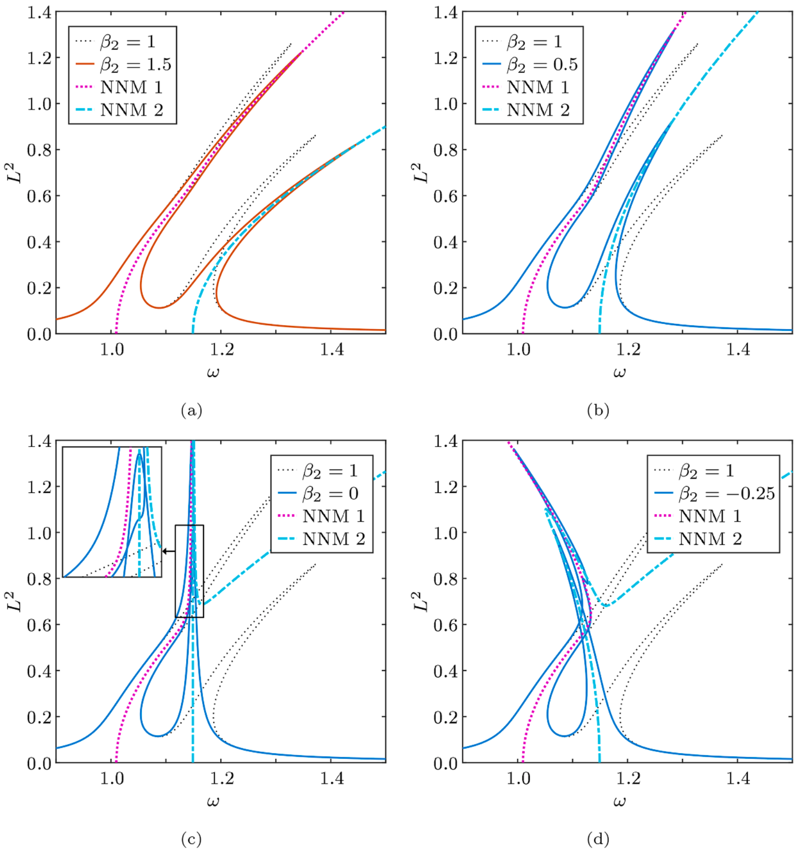

Fig. 3. Relation of the kinking effect to the system's nonlinearity, modified at oscillator 2. The reference curve for equal nonlinearity at both oscillators ($\beta_1 = \beta_2 = 1$) is shown as a black, dotted line. System response as the hardening stiffness coefficient is **(a)** increased (orange curve, $\beta_2 = 1.5$) and **(b)** reduced (blue curve, $\beta_2 = 0.5$). **(c)** System response as the nonlinear stiffness coefficient is removed (blue curve, $\beta_2 = 0$). The area of response branch intersection is shown as a close-up. Its aspect ratio is adapted to enhance visibility. **(d)** System response as a softening stiffness coefficient is introduced (blue curve, $\beta_2 = -0.25$). The frequency spacing constant for these graphs is $a = 0.3$. (For interpretation of the references to colour in this figure legend, the reader is referred to the web version of this article.)

3.3. Relation to the nonlinear stiffness coefficient

Now, we test whether the strength of the nonlinear stiffness coefficient affects the kinking phenomenon previously described. We distinguish between three cases: First, a stronger (or weaker) hardening stiffness, second, a linear oscillator with nonlinear stiffness removed, and third, a softening stiffness. Each are attained by modifying the nonlinear coefficient β at one oscillator. The results are presented in Fig. 3. In Figs. 3a, 3b, the variation of hardening stiffness shows that an increase of the coefficient causes the upward kink to flatten. A reduction shows the opposite effect, causing a more pronounced upward kink in the response. Removing the nonlinear stiffness altogether creates a linear second oscillator, cf. Fig. 3c. The resulting response curve shows vertical kinking as it approaches the linear oscillator's natural frequency. This causes the two resonant response branches to stack above each other. The vertical upward kink relates to veering in the NNMs. From the NNM trajectories, it can be seen that NNM 1 approaches NNM 2 and veers upward, avoiding a straight crossing through NNM 2. This behavior emerges in the forced response. The case of a softening stiffness is reported in Fig. 3d. As the onset of the second oscillator's resonance is approached, the upper response branch turns upward-and-leftward. It bends back toward lower frequencies as its amplitude increases. The resulting response curve looks as if the responses of a hardening and a softening Duffing oscillator are stacked on top of each other.

As observed, the system's nonlinearity affects the kink occuring in the system response. Stacking of the response branches is seen as an oscillator is made linear, and a backward bend was shown for a softening nonlinearity. Both effects cause an increase in response level compared to the case of identical nonlinearities.

3.4. Increasing model size

From the previous results, the question arises what happens as not only one, but multiple resonance overlaps occur for a given response branch. We expect additional kinks as resonance overlap extends over more than one oscillator. The system size is increased

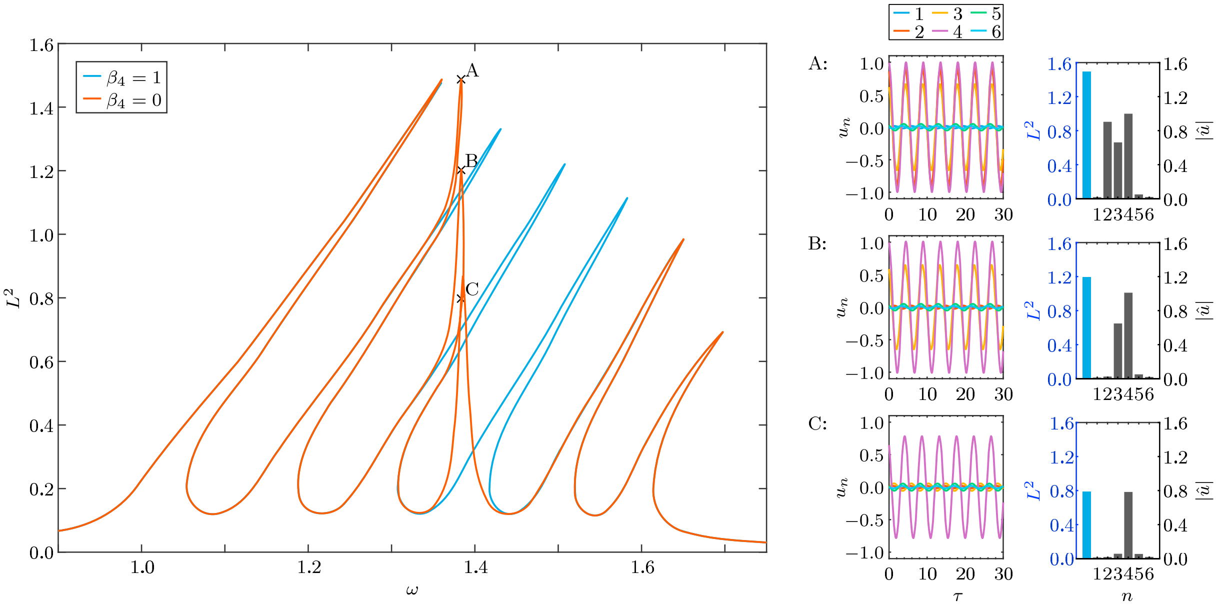

Fig. 4. Increase of system size to $N = 6$ oscillators, frequency spacing $a = 0.3$. Left panel: NFRCs for identical nonlinearities ($\beta_4 = \beta_n = 1$, blue curve) and a linear fourth oscillator ($\beta_4 = 0$, orange curve). Three points are marked A, B, C, corresponding to three solutions at the same frequency $\omega = 1.384$. Their time response analyses are displayed on the right side of the Figure. Middle panels show a section of the time responses, indicating stable periodic solutions. Right panels show the system's response levels and the oscillators' vibration amplitudes. (For interpretation of the references to colour in this figure legend, the reader is referred to the web version of this article.)

to a total of six oscillators. The frequency response curves are shown in Fig. 4 for two cases: identical nonlinearities (blue curve) as well as a linear oscillator 4 (orange curve, $\beta_4 = 0$). Multiple kinks for the upper response branches can be observed as they overlap the natural frequencies of the subsequent oscillators. This effect is best visible for the orange curve in Fig. 4, where the upper response branches show kinking before stacking as the linear oscillator is approached. In this setup, multiple response branches stack on top of each other. We now observe a narrow frequency band where multiple system states coexist at different response levels for a given frequency.

We compare three different response levels within the stacked frequency band. They are denoted, in descending level of response amplitude, A, B, C in Fig. 4. They all share the same frequency. Numerical time integration is performed over 500 periods to assess stability, shown in the middle panels of Fig. 4. All three points are found to be stable periodic solutions. The variation in system response level can be attributed to a localization effect in the vibration patterns. They are shown in the panels on the right-hand side of Fig. 4. For the highest response level (point A), oscillators 2, 3 and 4 show significant displacement and thus contribution. At point B, the vibration amplitude of oscillator 2 is significantly reduced. As a consequence, localization increases toward oscillators 3 and 4. For the lowest response level (point C), a reduction of displacement is observed for oscillator 3, thus localizing the vibration to oscillator 4 (the linear one).

It was shown that the addition of oscillators to the system creates additional kinks in the response branches as they overlap the natural frequencies of multiple subsequent oscillators. This extends to modifications of an oscillator's nonlinearity, as demonstrated for a linear oscillator in the chain. The resulting stacking phenomenon yields multiple stable solutions at different response levels, corresponding to localized vibration patterns.

To demonstrate the effect of a softening nonlinearity on the response curve in a multi-oscillator chain, a softening stiffness is introduced on the fourth oscillator. Fig. 5 shows three iterations of progressively stronger softening stiffness coefficients. A weakly softening spring (Fig. 5a, $\beta_4 = -0.1$) leads to backward bending of the response branches as the modified oscillator's natural frequency is approached. It imposes a limit on the frequency attainable by the bending response branches at around $\omega = 1.39$. These backward bends come with intersections between the branches; they fold over each other. This was already observed in the two-oscillator model (cf. Fig. 3d). Increasing the softening stiffness (Fig. 5b, $\beta_4 = -0.25$) results in more pronounced bends of the branches. This is accompanied by self-intersection of individual response branches in addition to intersections between neighboring branches. Further increase of the softening stiffness (Fig. 5C, $\beta_4 = -0.5$) shows an even stronger manifestation of this phenomenon. The curve now exhibits scissored sections, where the response drives back and forth in a large frequency range at high response levels.

As demonstrated, the backward bending effect observed in the system with two oscillators extends to a system of increased size. An effective frequency limit in the response is imposed beyond which the branches do not extend. As the strength of the softening stiffness is increased, complex phenomena unfold in the nonlinear frequency response. Self-intersections of individual response branches were found.

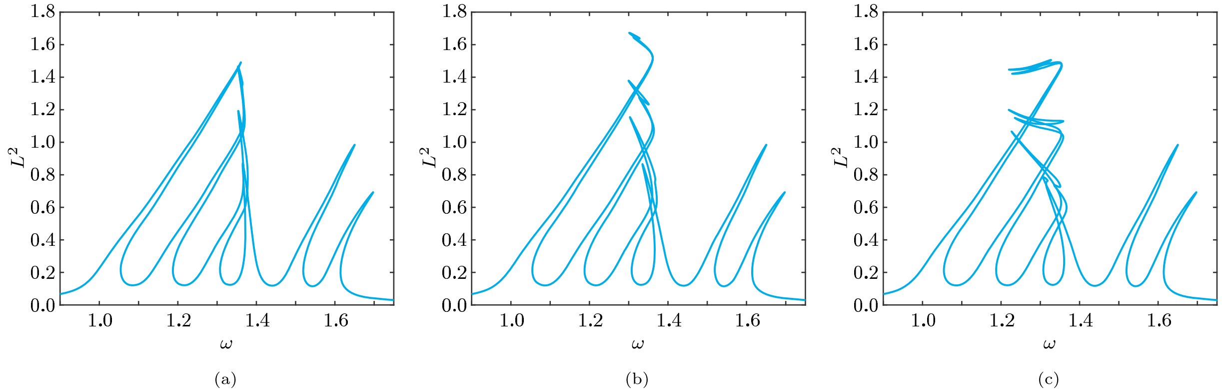

Fig. 5. System response for three different softening stiffness coefficients β at the fourth oscillator. **(a)** $\beta_4 = -0.1$, **(b)** $\beta_4 = -0.25$, **(c)** $\beta_4 = -0.5$. The parameters for these graphs are $N = 6$, $a = 0.3$.

3.5. *Nonlinear softening stiffness in the increased model*

In the previous section, it was shown that the frequency response exhibits complex behavior as the strength of softening nonlinearity increases. Regions of self-intersecting response branches were observed. Further investigation into related effects is performed on the system with softening stiffness $\beta_4 = -0.25$.

3.5.1. *Analysis of stability*

In this section, we assess stability of the response branches, focusing on the regions of self-intersection. The results are presented in Fig. 6a. As expected for systems with overhanging response curves, shadowed sections of the response branches are unstable. Bifurcation points indicate changes of stability. They mark turning points in the response curve. We note that no special bifurcation points are found at the points of self-intersection in the response. However, associated regions are found to be unstable. The corresponding branches remain unstable until after the self-intersection is resolved through another crossing point. Beyond the regions of self-intersection, parts of the response branch are found to contain stable solutions. These parts remain connected to the main branch through the self-intersecting (and unstable) regions, yet they may not be accessible through frequency sweeping. They appear semi-isolated relative to the main branch, forming *penisolas*. A Neimark-Sacker (NS) bifurcation is detected in the system, marked by a red asterisk in Fig. 6a. Here, a pair of complex conjugate Floquet exponents crosses the imaginary axis, taking on a positive real part. This is illustrated in the inset of Fig. 6a, where the system's Floquet exponents are shown for a point (i) just before and (ii) just after the Neimark-Sacker bifurcation. The periodic solution to the system becomes unstable, bifurcating into a Torus-like object. Continuation of the branch emanating from the NS point requires tracking of more than one frequency parameter [42]. A modified version of the Harmonic Balance method, often referred to as Multi-Harmonic Balance method (MHBM), has to be employed in this case. Implementations of MHBM are much less established than their single-frequency counterparts. Its application to track the system's Neimark-Sacker bifurcation is beyond the scope of this paper.

It was shown that the self-intersecting regions of the system response are unstable. They show no special bifurcation behavior. Semi-isolated sections containing stable solutions (or *penisolas*) were found.

3.5.2. *Nonlinear normal modes*

Next, we investigate the modal structure underlying the complex frequency response of the system with a softening stiffness ($\beta_4 = -0.25$). Nonlinear normal modes are computed. They are shown in Fig. 6b, including the NFRC. At a low response level, the modes start out according to their associated oscillators' backbone trajectories (i.e., mode 4 follows a softening backbone while the other modes follow a hardening one). As modes 1–3 increase their frequency with increasing amplitude, kinks can be observed. As the modal curves approach the natural frequency of the modified oscillator 4, they bend toward lower frequencies (these points are labelled "a" in Fig. 6b). The modes each trace the backbone of the softening oscillator for a section before turning back around as they meet another NNM (these points are labelled "b"). As the NNMs return toward higher frequencies, they initially reduce their response level before looping around (the loops are labelled "c"). After completing the loops, the NNMs bend backward again before turning around and back towards higher frequencies a second time (labelled "d"). The NNMs' response levels now drop down to a point where the NNMs converge to an original backbone curve (labelled "e"). We note that all points labelled "a" through "e" in Fig. 6b occur at points of internal resonance, where the NNM trajectories reach frequencies close to linear natural frequencies of the system. These interactions span a region we term zone of internal resonance. As the NNMs leave this zone, individual backbones become distinguishable again. A swap of modal trajectories is observed, where the NNMs now trace trajectories originally associated with other modes.

We have demonstrated complicated internal resonance effects in the system's NNMs. Backward bending encountered in the NFRC is observed in the NNMs as well. A zone of internal resonance is reported where NNMs with hardening and softening backbone curves interact, resulting in multiple turns, and loops.

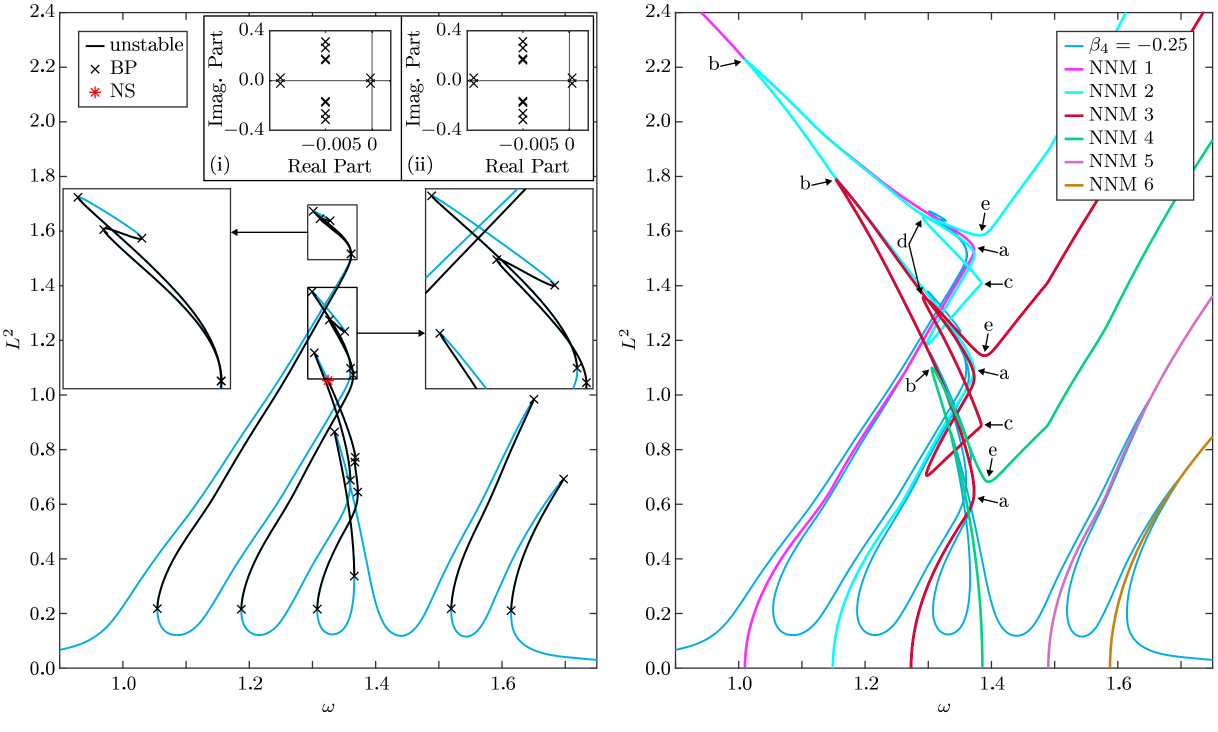

(a) (b)

Fig. 6. System response, softening stiffness coefficient at the fourth oscillator ($\beta_4 = -0.25$). Panel **(a)**: Stability analysis. Unstable sections are shown in black, bifurcation points are denoted by crosses. Regions with self-intersection of the response branches are shown as close-ups. Their aspect ratios have been adapted to enhance visibility. A Neimark-Sacker bifurcation is found on a backward bending branch around $\omega = 1.324$. The inset shows the Floquet exponents (i) just before and (ii) just after the NS bifurcation. Panel **(b)**: NNM analysis. The parameters for these graphs are $N = 6$, $a = 0.3$.

3.5.3. Variation of excitation amplitude

In the previous section, its was shown that the NNMs exhibit complicated, backward bending behavior. However, it was also found that the NNMs eventually return to the backbone trajectories of the individual oscillators. It would be expected that these parts of the NNMs become relevant in the forced response once the system's amplitude is increased.

To check this, we modify the excitation amplitude of the system. A stronger nonlinear response is expected from a stronger excitation, and thus, larger overhangs in the response curve are anticipated. Results are presented in Fig. 7, where the system's NFRC is shown for three different excitation levels. The blue curve shows a reduced excitation amplitude ($\hat{g}_n = 0.006$). It can be seen that the complex phenomena associated with the softening stiffness coefficient vanish as the excitation amplitude is reduced. The excitation is not strong enough to manifest internal resonances in the forced response. The orange curve ($\hat{g}_n = 0.012$) corresponds to the excitation level previously used for analysis of stability and NNMs, showing the already established backward bending and self-intersection phenomena. For the increased excitation level (yellow curve, $\hat{g}_n = 0.022$), multiple new phenomena emerge in the forced response. The softening backbone curve is now identified through the response branches. They align along the softening backbone trajectory. This results in a bent stacking effect of the branches. Most notably, the response branches at this excitation level overcome the frequency limit imposed through the softening oscillator's natural frequency and associated internal resonance. After bending backward, the branches now turn around to increase their frequency beyond the limiting frequency. The branches then come back toward lower frequencies again. This creates a swinging effect between high and low frequencies as the response level is gradually reduced. In doing so, the response branches follow the paths of the NNMs observed in the previous section, cf. Fig. 6b (for a reproduction of Fig. 7 with NNMs included, see Appendix B).

It was shown that an increase of excitation amplitude results in more pronounced bending effects. The response overcomes confinement to the zone of internal resonance, following the NNMs' backbone curves. A bent stacking effect is observed along the softening backbone trajectory, which becomes clearly distinguished.

4. Discussion

In this paper, we used a chain of nonlinear oscillators to examine the effect of neighboring oscillators on the system's response curve. We demonstrated a kinking effect in the response curve. It was related to the nonlinear normal modes of the system. We showed that kinking may be observed in the NNMs as well, attributed to a change in vibrational composition as internal 1:1 resonance occurs.

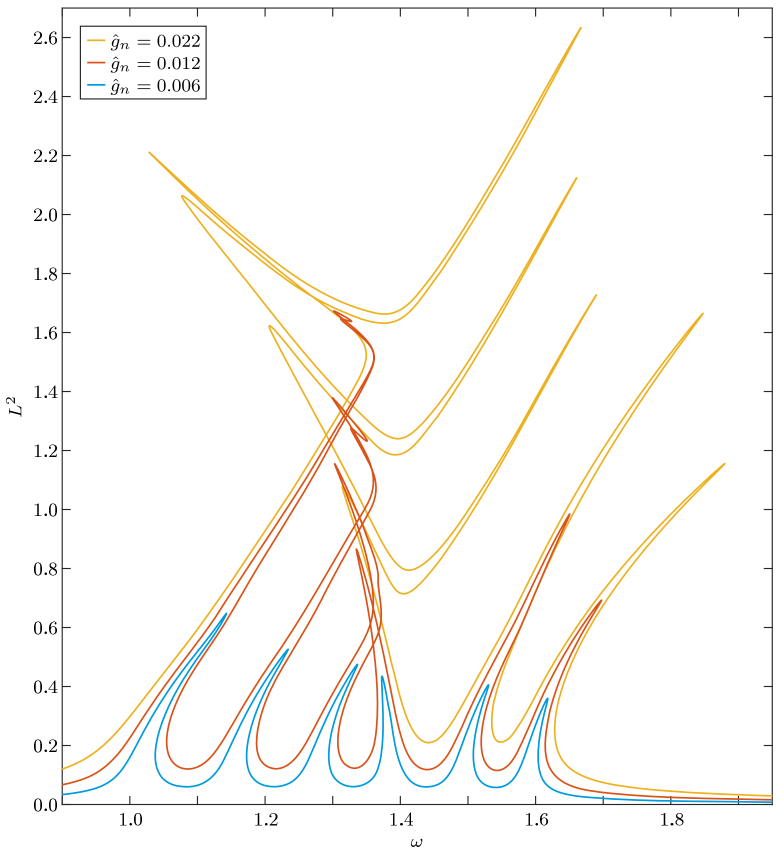

Fig. 7. System response for three levels of excitation amplitude: Reduced excitation amplitude (blue curve), regular excitation amplitude as used throughout this paper (orange curve), and increased excitation amplitude (yellow curve). For a reproduction of this Figure with NNMs included, the reader is referred to Appendix B. Parameters $N = 6$, $a = 0.3$, $\beta_4 = -0.25$. (For interpretation of the references to colour in this figure legend, the reader is referred to the web version of this article.)

These kinks emerged in the forced response once the system's natural frequencies became close enough so that resonance overlap was observed. By modifying the nonlinearity of neighboring oscillators, we demonstrated effects on the kinks in the response curve. Making an oscillator linear resulted in a vertical kinking effect where multiple response branches stacked on top of each other. Furthermore, we increased the system size, demonstrating multiple kinks in the response curve as multiple resonances were overlapped. Multiple solutions at different response levels were then found. These were shown to correspond to localized vibration patterns of the system. Finally, we introduced a softening stiffness at one oscillator in our model. The results showed a response curve with backward bends and self-intersection of response branches in a zone of internal resonance. Regions of self-intersection were found to be unstable, leading to sections of stable solutions becoming semi-isolated on a branch. As the system's excitation amplitude was increased, the forced response was driven further up along the backbone curves. The response branches effectively overcame an imposed frequency limit, leaving the zone of internal resonance to follow the original backbone trajectories.

Our results advance the understanding of frequency response in nonlinear dynamical systems. We analyzed the effect of neighboring oscillators on the response curve of the system. A relation between frequency spacing, oscillator nonlinearity and a kinking effect in the system's response curve was established. These results may be helpful in system design, where the offset of natural frequencies may be used to mitigate effects from internal resonance, or induce them. Additional oscillating components may be introduced to shape the response curve at designated frequencies by exploiting kinks. It should be possible to shape a system's response curve to ones liking as oscillators of various nonlinear properties are combined. In a suitable nonlinear system, it would be viable to reach a targeted response level at a certain frequency by introducing kinking through appropriately chosen add-on oscillators. Moreover, a frequency band of low response vibration may be created by introducing an appropriate (linear or maybe even softening) oscillator before said frequency, effectively creating a gap within the response curve. Modifications of excitation amplitude may be used to control the reach of response branches in resonance as they are driven up on the backbone curves of a system's nonlinear modes. Bends of the response branches may be initiated in a zone of internal resonance, which may be overcome as excitation amplitude is increased.

Our work motivates further research regarding nonlinear systems where kinking properties are observed. For example, it may be of interest to investigate an actual frequency sweep through such a system. One would expect the corresponding jump phenomena to take on interesting form as kinking, stacking and backward bending modify the response curve. Semi-isolated sections of the response may warrant special attention in this context. In addition, a detailed analysis of coordinate-wise responses may be of interest to increase the understanding of governing effects. It may also be worthwhile to take a closer look at the bifurcation structure of the model investigated. For example, the detected Neimark-Sacker bifurcation could be used as a starting point. Additional phenomena may be revealed with regard to kinking and stacking of response curves.

CRediT authorship contribution statement

Yannik Manz: Writing - review & editing, Writing - original draft, Visualization, Software, Methodology, Investigation, Formal analysis, Conceptualization; **André Gerlach:** Supervision, Project administration; **Norbert Hoffmann:** Writing - review & editing, Supervision, Conceptualization.

Declaration of competing interest

The authors declare that they have no known competing financial interests or personal relationships that could have appeared to influence the work reported in this paper.

Acknowledgments

The authors would like to thank Bernd Scheufele and Heiner Storck for valuable input during the preparation of the manuscript and for proof reading the article.

This work is partially funded by the Deutsche Forschungsgemeinschaft (DFG, German Research Foundation) – 671920 and under Germany's Excellence Strategy – EXC 3120/1 – 533771286.

Data availability

Data will be made available on request.

Appendix A. Eigenvalue problem of Hill's method for stability analysis: Coefficient matrices

The coefficient matrices $\boldsymbol{\Delta}_1$, $\boldsymbol{\Delta}_2$ from Eq. (13) are computed as

$$\begin{aligned}\boldsymbol{\Delta}_1 &= \boldsymbol{\nabla} \otimes 2\omega\mathbf{I} + \boldsymbol{\nabla}^0 \otimes \boldsymbol{\Xi},\\ \boldsymbol{\Delta}_2 &= \boldsymbol{\nabla}^0 \otimes \mathbf{I},\end{aligned} \tag{A.1}$$

where $\otimes$ denotes the Kronecker tensor product and $\boldsymbol{\nabla}$ is given as

$$\boldsymbol{\nabla} = \begin{bmatrix} 0 & & & & \\ & \ddots & & & \\ & & \boldsymbol{\nabla}_h & & \\ & & & \ddots & \\ & & & & \boldsymbol{\nabla}_H \end{bmatrix} \tag{A.2}$$

with

$$\boldsymbol{\nabla}_h = \begin{bmatrix} 0 & h \\ -h & 0 \end{bmatrix}, \quad h = 1 \dots H \tag{A.3}$$

Appendix B. Variation of excitation amplitude, including nonlinear normal modes

The following Fig. B.1 reproduces Fig. 7 with added nonlinear normal modes.

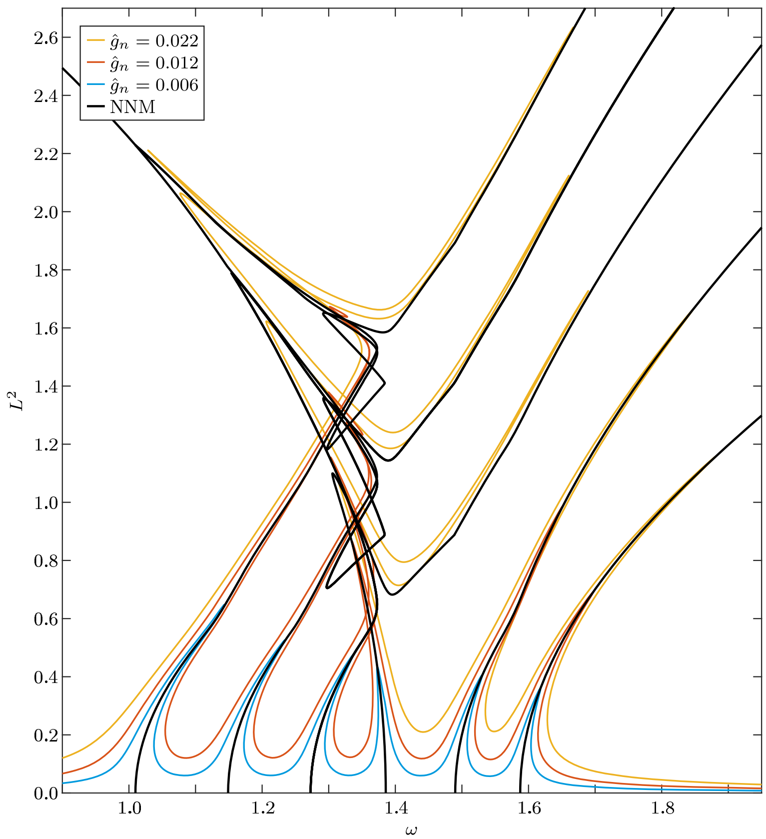

Fig. B.1. Reproduction of Fig. 7, including nonlinear normal modes. Note that all NNMs are shown in black to enhance visibility. For a better differentiation between individual NNM trajectories, refer to Fig. 6b.

References

[1] A.H. Nayfeh, D.T. Mook, Nonlinear Oscillations, Wiley, 1 edition, 1995. http://dx.doi.org/10.1002/9783527617586.

[2] G. Duffing, Erzwungene Schwingungen bei veränderlicher Eigenfrequenz und ihre technische Bedeutung (Forced Oscillations with Variable Natural Frequency and Their Technical Significance), Sammlung Vieweg, Vieweg, Braunschweig, Braunschweig, 1918.

[3] M. Krack, J. Gross, Harmonic Balance for Nonlinear Vibration Problems, Mathematical Engineering, Springer International Publishing, Cham, Cham, 2019. http://dx.doi.org/10.1007/978-3-030-14023-6.

[4] D.A. Ehrhardt, T.L. Hill, S.A. Neild, J.E. Cooper, Veering and nonlinear interactions of a clamped beam in bending and torsion, J. Sound Vib. 416 (2018) 1–16. http://dx.doi.org/10.1016/j.jsv.2017.11.045.

[5] D.A. Ehrhardt, T.L. Hill, S.A. Neild, Experimentally measuring an isolated branch of nonlinear normal modes, J. Sound Vib. 457 (2019) 213–226. http://dx.doi.org/10.1016/j.jsv.2019.06.006.

[6] S. Lenci, F. Clementi, Natural frequencies and internal resonance of beams with arbitrarily distributed axial loads, J. Appl. Comput. Mech. 7 (Special Issue) (2021) 1009–1019. http://dx.doi.org/10.22055/jacm.2020.32927.2104.

[7] S. Lenci, F. Clementi, L. Kloda, J. Warminski, G. Rega, Longitudinal–transversal internal resonances in timoshenko beams with an axial elastic boundary condition, Nonlinear Dyn. 103 (4) (2021) 3489–3513. http://dx.doi.org/10.1007/s11071-020-05912-z.

[8] Z. Chang, L. Hou, Y. Chen, Investigation on the 1:2 internal resonance of an FGM blade, Nonlinear Dyn. 107 (3) (2022) 1937–1964. http://dx.doi.org/10.1007/s11071-021-07070-2.

[9] X. Su, H. Kang, T. Guo, Y. Cong, Internal resonance and energy transfer of a cable-stayed beam with a tuned mass damper, Nonlinear Dyn. 110 (1) (2022) 131–152. http://dx.doi.org/10.1007/s11071-022-07644-8.

[10] M. Fu, O. Ameye, F. Yang, J. Košata, J. del Pino, O. Zilberberg, E. Scheer, Sideband attraction via internal resonance in a multimode membrane as a mechanism for frequency combs, Phys. Rev. Res. 7 (3) (2025) 033127. http://dx.doi.org/10.1103/3mtc-j9r9.

[11] S. Houri, D. Hatanaka, M. Asano, H. Yamaguchi, Demonstration of multiple internal resonances in a microelectromechanical self-sustained oscillator, Phys. Rev. Appl. 13 (1) (2020) 014049. http://dx.doi.org/10.1103/PhysRevApplied.13.014049.

[12] L. Ruzziconi, N. Jaber, L. Kosuru, M.L. Bellaredj, M.I. Younis, Internal resonance in the higher-order modes of a MEMS beam: experiments and global analysis, Nonlinear Dyn. 103 (3) (2021) 2197–2226. http://dx.doi.org/10.1007/s11071-021-06273-x.

[13] A. Opreni, M. Furlan, A. Bursuc, N. Boni, G. Mendicino, R. Carminati, A. Frangi, One-to-one internal resonance in a symmetric MEMS micromirror, Appl. Phys. Lett. 121 (17) (2022) 173501. http://dx.doi.org/10.1063/5.0120724.

[14] M. Zamanzadeh, H.G.E. Meijer, H.M. Ouakad, Internal resonance in a MEMS levitation force resonator, Nonlinear Dyn. 110 (2) (2022) 1151–1174. http://dx.doi.org/10.1007/s11071-022-07721-y.

[15] S. Azizi, H. Haddad Khodaparast, H. Madinei, M.I. Younis, G. Rezazadeh, Bifurcation-based dynamics and internal resonance in micro ring resonators for MEMS applications, Nonlinear Dyn. 113 (18) (2025) 24329–24342. http://dx.doi.org/10.1007/s11071-025-11379-7.

[16] O. Shoshani, S.W. Shaw, Resonant modal interactions in micro/nano-mechanical structures, Nonlinear Dyn. 104 (3) (2021) 1801–1828. http://dx.doi.org/10.1007/s11071-021-06405-3.

[17] K. Asadi, J. Yeom, H. Cho, Strong internal resonance in a nonlinear, asymmetric microbeam resonator, Microsyst. Nanoeng. 7 (1) (2021) 9. http://dx.doi.org/10.1038/s41378-020-00230-1.

[18] C. Liu, L. Li, Y. Zhang, Internal resonance of the coupling electromechanical systems based on josephson junction effects, Micromachines 13 (11) (2022) 1958. http://dx.doi.org/10.3390/mi13111958.

[19] L. Ruzziconi, N. Jaber, L. Kosuru, M.I. Younis, Activating internal resonance in a microelectromechanical system by inducing impacts, Nonlinear Dyn. 110 (2) (2022) 1109–1127. http://dx.doi.org/10.1007/s11071-022-07706-x.

[20] J. Yu, A. Donmez, H. Herath, H. Cho, One-to-two internal resonance in a micro-mechanical resonator with strong duffing nonlinearity, J. Micromech. Microeng. 34 (1) (2024) 015007. http://dx.doi.org/10.1088/1361-6439/ad0de8.

[21] A. Donmez, H. Herath, H. Cho, Theoretical insights into 1:2 and 1:3 internal resonance for frequency stabilization in nonlinear micromechanical resonators, Nonlinear Dyn. 113 (13) (2025) 15943–15962. http://dx.doi.org/10.1007/s11071-025-10987-7.

[22] B. Jin, Y. Bian, D. Tian, Z. Gao, An internal resonance based method for reducing torsional vibration of a gear system, Machines 10 (4) (2022) 269. http://dx.doi.org/10.3390/machines10040269.

[23] L.-Q. Chen, Y. Fan, Internal resonance vibration-based energy harvesting, Nonlinear Dyn. 111 (13) (2023) 11703–11727. http://dx.doi.org/10.1007/s11071-023-08464-0.

[24] J. Zhang, Y. Zhi, K. Yang, N. Hu, Y. Peng, B. Wang, Internal resonance characteristics of a bistable electromagnetic energy harvester for performance enhancement, Mech. Syst. Signal Process. 209 (2024) 111136. http://dx.doi.org/10.1016/j.ymssp.2024.111136.

[25] X. Wang, Z. Shi, Q. Yang, Y. Chen, X. Wei, R. Huan, Recent advancements of nonlinear dynamics in mode coupled microresonators: a review, Appl. Math. Mech. 46 (2) (2025) 209–232. http://dx.doi.org/10.1007/s10483-025-3211-6.

[26] R.H. Plaut, N. HaQuang, D.T. Mook, The influence of an internal resonance on non-linear structural vibrations under two-frequency excitation, J. Sound Vib. 107 (2) (1986) 309–319. http://dx.doi.org/10.1016/0022-460X(86)90240-3.

[27] A.I. Manevitch, L.I. Manevitch, Free oscillations in conservative and dissipative symmetric cubic two-degree-of-freedom systems with closed natural frequencies, Meccanica 38 (3) (2003) 335–348. http://dx.doi.org/10.1023/A:1023362112580.

[28] A. Grolet, F. Thouverez, Computing multiple periodic solutions of nonlinear vibration problems using the harmonic balance method and groebner bases, Mech. Syst. Signal Process. 52–53 (2015) 529–547. https://dx.doi.org/10.1016/j.ymssp.2014.07.015.

[29] F. Mangussi, D.H. Zanette, Internal resonance in a vibrating beam: a zoo of nonlinear resonance peaks, Plos One 11 (9) (2016) e0162365. http://dx.doi.org/10.1371/journal.pone.0162365.

[30] D. Hong, T.L. Hill, S.A. Neild, Existence and location of internal resonance of two-mode nonlinear conservative oscillators, Proc. R. Soc. A: Math. Phys. Eng. Sci. 478 (2260) (2022) 20210659. http://dx.doi.org/10.1098/rspa.2021.0659.

[31] G. Kerschen, M. Peeters, J.C. Golinval, A.F. Vakakis, Nonlinear normal modes, part i: a useful framework for the structural dynamicist, Mech. Syst. Signal Process. 23 (1) (2009) 170–194. http://dx.doi.org/10.1016/j.ymssp.2008.04.002.

[32] F. Clementi, S. Lenci, G. Rega, 1:1 Internal resonance in a two d.o.f. complete system: a comprehensive analysis and its possible exploitation for design, Meccanica 55 (6) (2020) 1309–1332. http://dx.doi.org/10.1007/s11012-020-01171-9.

[33] S. Tatzko, Internal resonance in nonlinear structures—and what it can be used for, PAMM 23 (3) (2023) e202300210. http://dx.doi.org/10.1002/pamm.202300210.

[34] A. Papangelo, F. Fontanela, A. Grolet, M. Ciavarella, N. Hoffmann, Multistability and localization in forced cyclic symmetric structures modelled by weakly-coupled duffing oscillators, J. Sound Vib. 440 (2019) 202–211. http://dx.doi.org/10.1016/j.jsv.2018.10.028.

[35] S. Quaegebeur, N. Di Palma, B. Chouvion, F. Thouverez, Exploiting internal resonances in nonlinear structures with cyclic symmetry as a mean of passive vibration control, Mech. Syst. Signal Process. 178 (2022) 109232. http://dx.doi.org/10.1016/j.ymssp.2022.109232.

[36] X. Jin, C.G. Baker, E. Romero, N.P. Mauranyapin, T.M.F. Hirsch, W.P. Bowen, G.I. Harris, Engineering error correcting dynamics in nanomechanical systems, Sci. Rep. 14 (1) (2024) 20431. http://dx.doi.org/10.1038/s41598-024-71679-7.

[37] M. Bonhage, J.T. Adler, C. Kolhoff, O. Hentschel, K.-D. Schlesier, L.P.-v. Scheidt, J. Wallaschek, Transient amplitude amplification of mistuned structures: an experimental validation, J. Sound Vib. 436 (2018) 236–252. http://dx.doi.org/10.1016/j.jsv.2018.07.031.

[38] L. Ouyang, H. Shang, H. Chen, Q. Bi, L.-M. Zhu, The mechanism on prediction of transient maximum amplitude for tuned and mistuned blisks, J. Eng. Gas Turbines Power 142 (5) (2020) 051013. http://dx.doi.org/10.1115/1.4046761.

[39] B. Niedergesäß, A. Papangelo, A. Grolet, A. Vizzaccaro, F. Fontanela, L. Salles, A.J. Sievers, N. Hoffmann, Experimental observations of nonlinear vibration localization in a cyclic chain of weakly coupled nonlinear oscillators, J. Sound Vib. 497 (2021) 115952. http://dx.doi.org/10.1016/j.jsv.2021.115952.

[40] C. Geier, M. Stender, N. Hoffmann, Building functional networks for complex response analysis in systems of coupled nonlinear oscillators, J. Sound Vib. 590 (2024) 118544. http://dx.doi.org/10.1016/j.jsv.2024.118544.

[41] C. Geier, N. Hoffmann, Exploring localization in nonlinear oscillator systems through network-based predictions, Chaos: Interdiscip. J. Nonlinear Sci. 35 (5) (2025) 053126. http://dx.doi.org/10.1063/5.0265366.

[42] R. Seydel, Practical Bifurcation and Stability Analysis, 5 of *Interdisciplinary Applied Mathematics*, Springer New York, New York, NY, New York, NY, 2010. http://dx.doi.org/10.1007/978-1-4419-1740-9.

[43] S. Engelnkemper, S.V. Gurevich, H. Uecker, D. Wetzel, U. Thiele, Continuation for thin film hydrodynamics and related scalar problems, in: A. Gelfgat (Ed.), Computational Modelling of Bifurcations and Instabilities in Fluid Dynamics, 50, Springer International Publishing, Cham, 2019, pp. 459–501. http://dx.doi.org/10.1007/978-3-319-91494-7_13.

[44] E.L. Allgower, K. Georg, Numerical Continuation Methods, 13 of *Springer Series in Computational Mathematics*, Springer Berlin Heidelberg, Berlin, Heidelberg, Berlin, Heidelberg, 1990. http://dx.doi.org/10.1007/978-3-642-61257-2.

[45] E.J. Doedel, AUTO: A program for the automatic bifurcation analysis of autonomous systems, Congr.Numer 30 (1981) 265–284.

[46] A. Dhooge, W. Govaerts, Yu.A. Kuznetsov, MATCONT: A MATLAB package for numerical bifurcation analysis of ODEs, ACM Trans. Math. Softw. 29 (2) (2003) 141–164. https://dx.doi.org/10.1145/779359.779362.

[47] MANLAB, 2011, (https://manlab.lma.cnrs-mrs.fr/spip/).

[48] A.F. Vakakis, NON-LINEAR NORMAL MODES (NNMs) AND THEIR APPLICATIONS IN VIBRATION THEORY: AN OVERVIEW, Mech. Syst. Signal Process. 11 (1) (1997) 3–22. http://dx.doi.org/10.1006/mssp.1996.9999.

[49] R.M. Rosenberg, Normal modes of nonlinear dual-mode systems, J. Appl. Mech. 27 (2) (1960) 263–268. http://dx.doi.org/10.1115/1.3643948.

[50] R.M. Rosenberg, The normal modes of nonlinear N-degree-of-freedom systems, J. Appl. Mech. 29 (1) (1962) 7–14. http://dx.doi.org/10.1115/1.3636501.

[51] R.M. Rosenberg, On nonlinear vibrations of systems with many degrees of freedom, in: Advances in Applied Mechanics, 9, Elsevier, 1966, pp. 155–242. http://dx.doi.org/10.1016/S0065-2156(08)70008-5.

[52] S.W. Shaw, C. Pierre, Non-linear normal modes and invariant manifolds, J. Sound Vib. 150 (1) (1991) 170–173. http://dx.doi.org/10.1016/0022-460X(91)90412-D.

[53] S.W. Shaw, C. Pierre, Normal modes for non-linear vibratory systems, J. Sound Vib. 164 (1) (1993) 85–124. http://dx.doi.org/10.1006/jsvi.1993.1198.

[54] S.W. Shaw, C. Pierre, Normal modes of vibration for non-linear continuous systems, J. Sound Vib. 169 (3) (1994) 319–347. http://dx.doi.org/10.1006/jsvi.1994.1021.

[55] M. Peeters, R. Viguié, G. Sérandour, G. Kerschen, J.C. Golinval, Nonlinear normal modes, part II: toward a practical computation using numerical continuation techniques, Mech. Syst. Signal Process. 23 (1) (2009) 195–216. http://dx.doi.org/10.1016/j.ymssp.2008.04.003.

[56] G. Von Groll, D.J. Ewins, THE HARMONIC BALANCE METHOD WITH ARC-LENGTH CONTINUATION IN ROTOR/STATOR CONTACT PROBLEMS, J. Sound Vib. 241 (2) (2001) 223–233. https://dx.doi.org/10.1006/jsvi.2000.3298.

[57] T. Detroux, L. Renson, L. Masset, G. Kerschen, The harmonic balance method for bifurcation analysis of large-scale nonlinear mechanical systems, Comput. Methods Appl. Mech. Eng. 296 (2015) 18–38. https://dx.doi.org/10.1016/j.cma.2015.07.017.

[58] G. Moore, Floquet theory as a computational tool, SIAM J. Numer. Anal. 42 (6) (2005) 2522–2568. http://dx.doi.org/10.1137/S0036142903434175.
[59] P. Ribeiro, M. Petyt, Non-linear free vibration of isotropic plates with internal resonance, Int. J. Non-Linear Mech. 35 (2) (2000) 263–278. http://dx.doi.org/10.1016/S0020-7462(99)00013-X.
[60] MATLAB Version 24.2.0.2712019 (R2024b), Natick, Massachusetts, 2024.